Sensor-based Navigation of Air-duct Inspection Mobile Robots

K. C. Koh[a], H. J. Choi[a], J. S. Kim[a], K.W. Ko[b], and H. S. Cho[b]

[a]Department of Mechanical and Control Engineering, Sunmoon University
[b]Department of Mechanical Engineering, Korea Advanced Institute of Science and Technology

ABSTRACT

This paper deals with an image sensor system and its position estimation algorithm for autonomous duct cleaning and inspection mobile robots. For the real application, a hierarchical control structure that consists of robot motion controller and image sensor system is designed considering the efficient and autonomous motion behaviors in narrow space such as air ducts. The sensor system consists of a *CCD* camera and two laser sources to generate slit beams. The image of the structured lights is used for calculating the geometric parameters of the air ducts which are usually designed with a rectangular section. With the acquired *3D* information about the environment, the mobile robot with two differential driving wheels is able to autonomously navigates along the duct path without any human intervention. For real time navigation, the relative position estimation of the robot are performed from *3D* image reconstructed by the sensor system. The calibration and image processing methods used for the sensor system are presented with the experimental data. The experimental results show the possibility of the sensor based navigation which is important for effective duct cleaning by small mobile robots.

Keywords: mobile robot, image sensor , position estimation, navigation, duct cleaning

1. INTRODUCTION

Recently, application areas of small mobile robots are being extended to service industry including the cleaning in office, surveillance, the duct cleaning and inspection. In particular, the air pollution of the large buildings or vast underground public areas as subway lobby causes the serious environmental problems. The cleaning robots for air ducts are used to maintain the air ventilation system sanitary. Most of commercialized duct cleaning robots are controlled by manual operation using visual information which degrades the human control ability and cleaning efficiency in narrow and long space. In this study, in order to improve the limitation of the manually operated duct cleaning robots, an image sensor system using structured laser sources is developed for autonomous mobile navigation. The position estimation problem of mobile robots has been the long-time issues and various methods have been introduced by the previous research works[1]-[3] which include the methods using artificial land marks methods[1], beacons[2] and others[3]. The artificial land mark has difficulty of application in the pollutive air duct and the sonar sensor has the limitation in the measurement accuracy. The paper presents a position estimation method using the structured light vision which provides the three-dimensional surface information about the air duct. For real application, the prototype of the air duct inspection and cleaning robot is designed and the effectiveness of the proposed method is demonstrated via a series of position estimation experiments. The results show the possibility of the practical use in the efficient duct cleaning process.

The organization of the paper is as follows. In section 2, we introduce a mobile robot for cleaning and inspection of air ducts. In section 3, we describe a sensor system developed for the autonomous navigation of the robot. In section 4, the algorithms of the image processing and position estimation are presented in detail and results of a series of experimental tests are given. Finally, some conclusions are made in the last section.

2. DESIGN OF DUCT ROBOT(INCRA I)

In this section, the mechanical and control structures of the prototype duct robot are described. The robot is designed to autonomously navigate and measure the pollution amount in the air duct. Fig. 1 shows overview of the robot named INCRA

Optomechatronic Systems, Hyungsuck Cho, George K. Knopf, Editors,
Proceedings of SPIE Vol. 4190 (2001) © 2001 SPIE · 0277-786X/01/$15.00

I (INspection and Cleaning Robot for Air duct of version I) which is equipped with a CCD camera and controlled by a personal computer which generates the wheel velocity commands by processing the visual image. INCRA I has four wheel drive mechanism. The fore and left wheel is driven by another DC servo motor and also connected to the rear and left wheel by a mechanical link. The other side, the rear and right wheel is driven by a DC servo motor and connected to the fore and right wheel. Thus, the robot has the similar mobility as the differential wheel driven robot. On the top of the robot, a pan and tilt mechanism gives the camera two degrees of freedom.

The robot controller consists of a command controller(CC), a wheel controller(WC) and a mount controller(MC). CC processes the analysis of the sensor information and generates control commands for WC and MC. WC controls the wheel velocities and reports the control results by the encoder values to MC. MC controls motion of the camera mount and transmits the image information to CC. Fig.2 shows the hierarchical structure of the robot controller. The wheel driving motors have the optical encoders at each rotational axis and their velocities are controlled by WC which is based on *80C196KC* micro controller

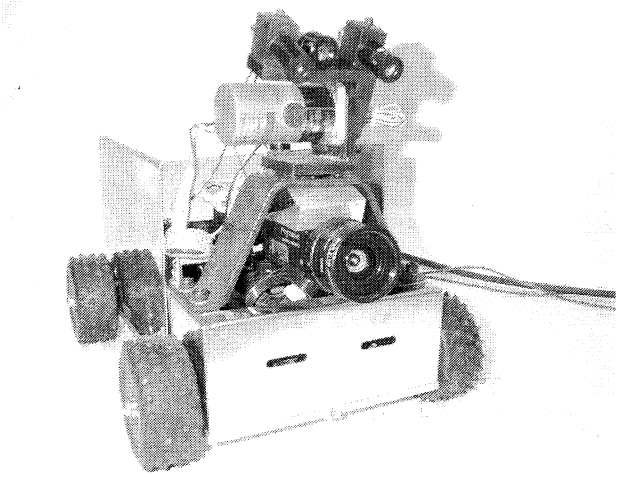

Fig.1 INCRA I

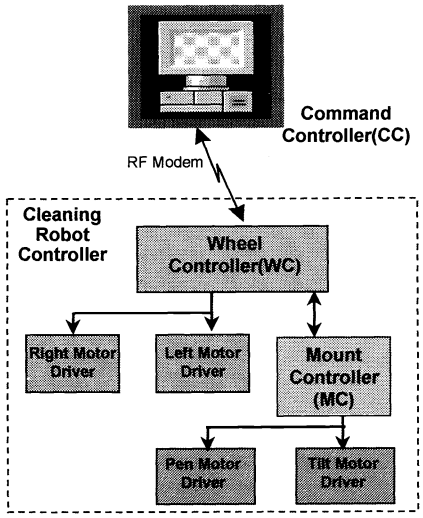

Fig.2 Control Structure

3. IMAGE SENSOR SYSTEM

The anatomy of the mobile robot navigation is very important for efficient operation in narrow space such as air duct. For this end, it is necessary to design the sensor system and develop the localization algorithm for the mobile robot. In the study, we consider a laser range finder consisting of a CCD camera and two slit beam laser sources. The camera is the SONY-XC55, non-interlace 640*480 CCD camera. The position estimation relative to the air duct is performed by using the three dimensional information acquired by slit-beam laser and a CCD camera. Fig.3 shows the principle of the 3D object recognition using the structured laser beams. Since the structured lighting approach is relatively well known, only an overview of the methodology is briefly presented here.

The fixed coordinates *OXYZ* denote the camera coordinates, the 2D coordinates *UV* denote the pixel coordinates on digital image plane, and the $X'Y'$ is defined as the image plane coordinates. Specifically, to compute the 3D coordinates(*x, y, z*) of any point on the laser strip from the 2D coordinates (*u, v*), a transformation T(4x3 matrix) relates the pixel coordinates to the camera coordinates by the following homogeneous coordinates transform,

$$s[x,y,z,1]^T = T_S^U [u,v,1]^T \tag{1}$$

where s is the scaling factor of the homogeneous transform and T_S^U is the perspective transform matrix from pixel coordinates to camera coordinates. The matrix T_S^U can be theoretically obtained from the geometrical analysis on Fig.3.

L_x is the vertical field of view of the camera at depth T which denotes the maximum measuring distance in Z direction. θ denotes the separation angle of laser slit beam, and f is the focal length of the camera lens. The distance D denotes base line between camera and laser diode and is given by

$$D = T / \tan\theta - L_x / 2 . \tag{2}$$

Let α be the field angles of camera view on Y' and then, L_x is followed by

$$L_x = 2\tan(\alpha / 2) / T \tag{3}$$

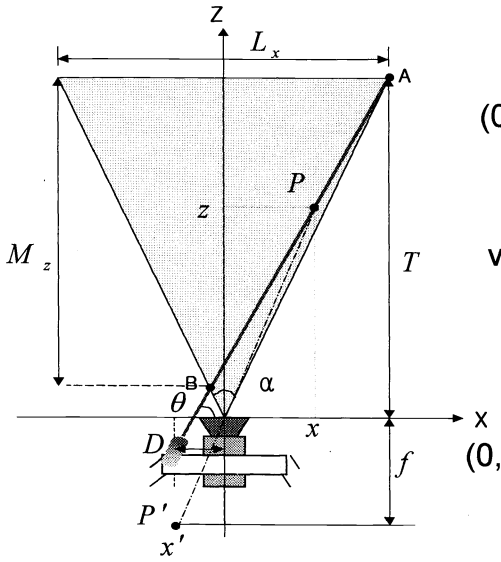

Fig.3 Principle of 3D object recognition using the structured laser

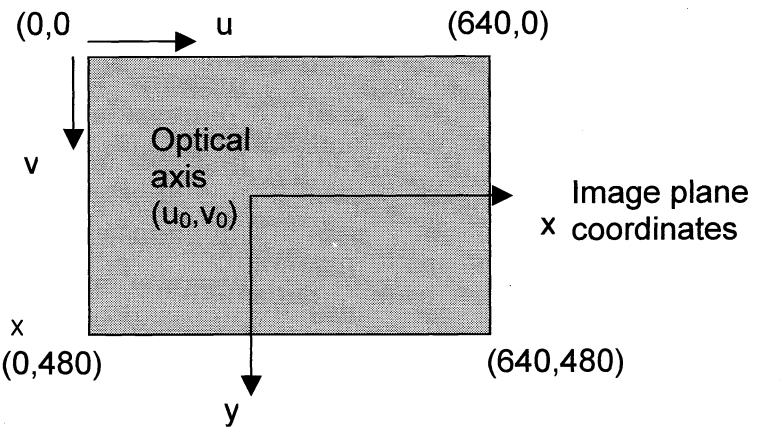

Fig.4 Pixel coordinates

A stripe point P on the line AB uniquely corresponds to a point P' on the image plane. Thus the following equation is satisfied by the geometric relations shown in Fig.3.

$$z = (D + x)\tan\theta \tag{4}$$

We let $1''$ be the projective point on image plane of P. From triangulation, the relation between image coordinates and the camera coordinates are given by

$$\frac{x}{z} = \frac{x'}{f} \tag{5}$$

$$\frac{y}{z} = \frac{y'}{f} . \tag{6}$$

From(4) and (5), the x coordinates of a stripe point P is given by

$$x = \frac{x' D \tan\theta}{f - x' \tan\theta} \tag{7}$$

and by applying (5) to (7), we can obtain

$$z = \frac{fD \tan\theta}{f - x' \tan\theta}. \tag{8}$$

Then, by substituting (8) into (6), the following equation can be acquired.

$$y = \frac{y' D \tan\theta}{f - x' \tan\theta}. \tag{9}$$

(7), (8) and (9) can be written by the following matrix form.

$$s\begin{bmatrix} x \\ y \\ z \\ 1 \end{bmatrix} = \begin{bmatrix} 1 & 0 & 0 \\ 0 & 1 & 0 \\ 0 & 0 & f \\ -1/D & 0 & f/D\tan\theta \end{bmatrix}\begin{bmatrix} x' \\ y' \\ 1 \end{bmatrix}. \tag{10}$$

As shown in Fig.4, the relationship between the pixel coordinates and the image plane coordinates is given by the following homogeneous transformation

$$\begin{bmatrix} u \\ v \\ 1 \end{bmatrix} = \begin{bmatrix} k_u & 0 & u_0 \\ 0 & k_v & v_0 \\ 0 & 0 & 1 \end{bmatrix}\begin{bmatrix} x' \\ y' \\ 1 \end{bmatrix} \tag{11}$$

where k_u and k_v are scale factor between the pixel values and image coordinates with unit of pixels/m which determine the image resolution, and u_0 and v_0 are the offset values on pixel coordinates. From (10) and (11), the perspective transformation matrix T_S^U can be obtained as

$$T_S^U = \begin{bmatrix} 1 & 0 & 0 \\ 0 & 1 & 0 \\ 0 & 0 & f \\ -1/D & 0 & f/D\tan\theta \end{bmatrix}\begin{bmatrix} k_u & 0 & u_0 \\ 0 & k_v & v_0 \\ 0 & 0 & 1 \end{bmatrix}^{-1} = \begin{bmatrix} 1/k_u & 0 & -u_0/k_u \\ 0 & 1/k_v & -v_0/k_v \\ 0 & 0 & f \\ -1/Dk_u & 0 & -u_0/Dk_u + f/D\tan\theta \end{bmatrix}. \tag{12}$$

In real application, the coefficients of T_S^U in (12) are determined via camera calibration process since they are often difficult to accurately obtain due to lens distortion or structural uncertainties in camera optics. Therefore, the matrix T_S^U is computed off-line during the camera and projector calibration process by observing the known feature points in camera coordinates and extracting the laser stripes by using the accurately machined block gauge as shown in Fig.4. Since the scaling factor can be set by any value, t_{43} can be made *1* by

$$s\begin{bmatrix} x \\ y \\ z \\ 1 \end{bmatrix} = \begin{bmatrix} t_{11} & t_{12} & t_{13} \\ t_{21} & t_{22} & t_{21} \\ t_{31} & t_{32} & t_{33} \\ t_{41} & t_{42} & 1 \end{bmatrix} \begin{bmatrix} u \\ v \\ 1 \end{bmatrix}. \tag{13}$$

By rearranging (13) for t_{ij}, the following equation can be written.

$$\begin{bmatrix} u^1 & v^1 & 1 & 0 & 0 & 0 & 0 & 0 & 0 & -u^1x_s^1 & -v^1x_s^1 \\ 0 & 0 & 0 & u^1 & v^1 & 1 & 0 & 0 & 0 & -u^1y_s^1 & -v^1y_s^1 \\ 0 & 0 & 0 & 0 & 0 & 0 & u^1 & v^1 & 1 & -u^1z_s^1 & -v^1z_s^1 \\ \vdots & \vdots & \vdots & \vdots & \vdots & \vdots & \vdots & \vdots & \vdots & \vdots & \vdots \\ u^n & v^n & 1 & 0 & 0 & 0 & 0 & 0 & 0 & -u^nx_s^n & -v^nx_s^n \\ 0 & 0 & 0 & u^n & v^n & 1 & 0 & 0 & 0 & -u^ny_s^n & -v^ny_s^n \\ 0 & 0 & 0 & 0 & 0 & 0 & u^n & v^n & 1 & -u^nz_s^n & -v^nz_s^n \end{bmatrix} \begin{bmatrix} t_{11} \\ t_{12} \\ t_{13} \\ t_{21} \\ t_{22} \\ t_{23} \\ t_{31} \\ t_{32} \\ t_{33} \\ t_{41} \\ t_{42} \end{bmatrix} = \begin{bmatrix} x_s^1 \\ y_s^1 \\ z_s^1 \\ \vdots \\ x_s^n \\ y_s^n \\ z_s^n \end{bmatrix} \tag{14}$$

where x_s^i, y_s^i, z_s^i and u^i, v^i are the camera coordinates and their corresponding pixel coordinates for the known test feature points, respectively. Since the matrix T_S^U involves 11 unknown coefficients as in as (13), at least *4* feature points which do not exist on a same plane are needed for the calibration. In the study, *9* feature points are extracted by varying the camera position in z-direction towards a block gauge as in Fig.5.

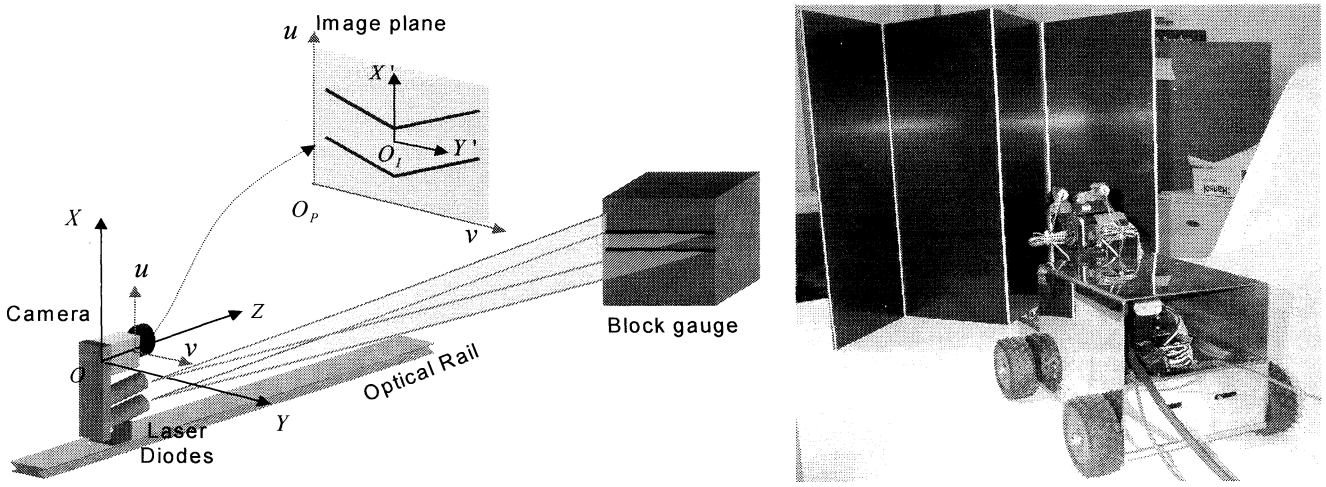

Fig.5 Camera Calibration

In table 1, the results of the camera calibration are summarized.

4. POSITION ESTIMATION

4.1 Image processing algorithm

The image processing algorithm is to extract laser stripe data from acquired images which may contain other possible bright sources such as the reflection of laser light from the unknown specular objects. The most reliable feature for extracting laser stripe is thickness of laser stripe in the image plane. The basic idea of robust extraction of laser stripe is to find the highlighted object which has a known thickness of laser stripe in an acquired image. The thickness of laser stripe slightly changes depending on the distance from target to laser source. The image in the corner is slightly blurred and thus thickness of laser stripe also changes because the focal depth of camera lens has a little limitation to cover all the range. To extract two 3D line equations from the image, the several prep-processing algorithms are sequentially performed. At first, a binary image is obtained by thresholding the gray level image, and noises are rejected by morphology expansion and reduction algorithm. Then, line masks used for thining the binary image are obtained by measuring the thickness of binary laser images, and the parameters(r, θ) of the line equations are determined by applying the Hough transform. The 2D points on the lines are transformed to the corresponding 3D points by Eq. (9). The four 3D points compose two 3D lines which are used for making 3D plane explained in section 4.2. Fig.6 shows the S/W flow chart for the image pre-processing.

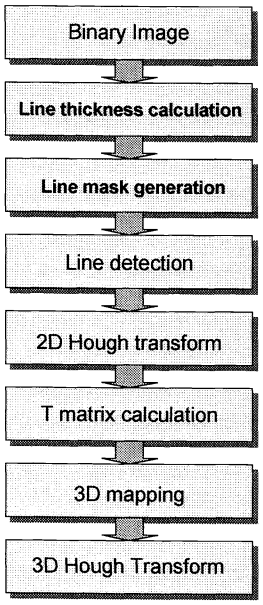

Fig.6 Flow chart of pre-processing algorithm

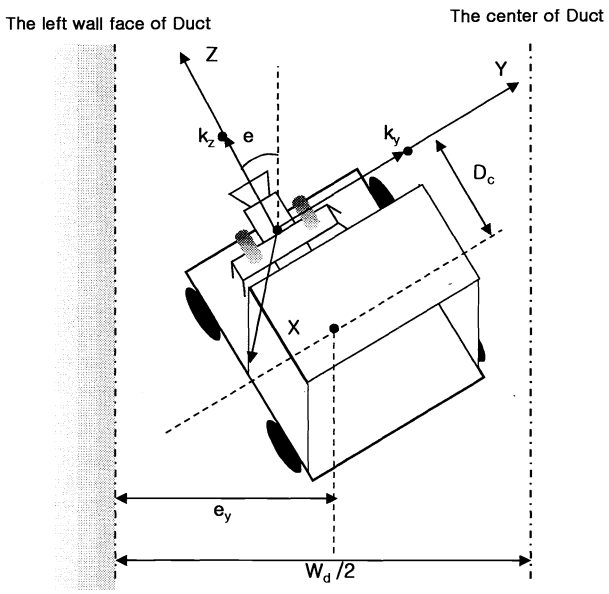

Fig.7 Position estimation relative to duct

4.2 Position estimation algorithm

The interior of the air duct has the structured environment composed of several planes. When two laser stripes are projected on a plane, two straight are projected on a plane, two straight lines appear in image plane as shown in Fig.4. Generally, the line equation in *3D* space is as follows

$$\frac{x-a_1}{b_1}=\frac{y-a_2}{b_2}=\frac{z-a_3}{b_3},$$

$$\vec{x}=\vec{a}+t\cdot\vec{b} \qquad (15)$$

where $\vec{a}$ is the position vector and $\vec{b}$ is the directional vector. Two straight lines in image plane can be detected by Hough transform[5]. Using the acquired line equation in 2D image plane and Eq.(1), the 3D line equation can be acquired easily. Let the acquired 3D line equations be L_1 and L_2. From Eq.(10), these lines are represented as follows:

$$L_1 : \vec{x} = \vec{g}_1 + t \cdot \vec{h}_1, \qquad L_2 : \vec{x} = \vec{g}_2 + t \cdot \vec{h}_2 \tag{16}$$

where $\vec{h}_1$ and $\vec{h}_2$ are the directional vectors for L_1 and L_2, respectively. Generally, the plane equation in 3D spaces and its vector form are given by

$$\vec{x} \cdot \vec{k} - d = 0 \tag{17}$$

where $\vec{k}$ is normal vector of the plane d is the distance from origin to the plane. In the case that the L_1 and L_2 lie on the same plane P_1, the two directional vectors, $\vec{h}_1$ and $\vec{h}_2$ make the normal vector by the following equation,

$$\vec{k} = \vec{h}_1 \times \vec{h}_2 . \tag{18}$$

If Eq.(11) is substituted to Eq.(12), d can be calculated.

4.3 Experimental results and discussion

To observe the effectiveness of the position estimation method, a series of experimental tests are conducted for the prototype robot INCRA I working in a real air duct. For different locations around the measurement gauge, the position estimation of the robot is performed. Table 2 and 3 show the experimental results. By use of the proposed method, four geometrical parameters (k_x, k_x, k_x, d) of the planar equation can be on-line determined and the heading angle error, e_θ and the lateral path error, e_y are used for path tracking algorithm[7] to be studied hereafter using

$$e_y = W_d / 2 - D_c \sin e_\theta - d \tag{19}$$

$$e_\theta = \tan^{-1}(k_z / k_y) \tag{20}$$

where W_d is the duct width and D_c is offset distance between the center of camera and the center of robot(see Fig.7). The experimental results of Fig.8 show that the position estimation is useful for the autonomous navigation in real time.

5. CONCLUSION

In this paper, we presented the position estimation of the mobile robot working in the air duct for cleaning and inspection. A sensor system using two laser stripes and a CCD camera was developed to estimate the robot position relative to the wall of the duct and to recognize the 3D shape of the duct surface. The control structure for the robot was described and image processing algorithms including pre-processing were considered. Through the experimental tests, the effectiveness of the proposed position estimation method was evaluated. The experimental results show the applicability of the method for autonomous navigation of the mobile robot in air duct. Now, we are performing the path tracking tests for various shapes of the air ducts.

6. ACKNOWLEGEMENTS

This work was supported by the Korea Science and Engineering Foundation(KOSEF) through the RRC-ACCT at Sunmoon University.

7. REFERENCES

1. K. C. Koh, J. S. Kim and H. S. Cho, "A position estimation system for mobile robots using a monocular image of a 3-D landmark," Robotica, Vol. 12, pp.431-441, 1994.
2. M. Julliere, L. Marce and H. Place, "A Guidance System for a Mobile Robot", Proc. 13th Int. Symp. On Industrial Robots, pp.58-68, 1983.
3. T. Hongo, H. Arkawa et al., "An Automatic Guidance System of a Self-controlled Vehicle", IEEE Trans. Ind. Elec. IE-34, No. 1, pp.5-10, 1987
4. J. S. Kim and H. S. Cho, "A robust visual seam tracking system for robotic arc welding", Mechatronics, Vol.6, No.2, pp.141-163, 1996.
5. D. H. Ballard, C. M. Brown, Computer vision, Prentice Hall, 1982.
6. E. R. Davis, Machine Vision: Theory, Algorithms and Practicalities, Academic Press, 1997.
7. K. C. Koh and H. S. Cho, "A Smooth Path Tracking Algorithm for Wheeled Mobile Robots, J. of Intelligent and Robotic Systems," Vol.24, pp. 367-385, 1999.
8. Borenstein and Y. Koren, "Motion control analysis of a mobile robot," ASME J. of Dynamic Systems Measurement and Control, vol. 109, pp. 73-79, 1987.
9. I. J. Cox, "Blanche-An experiment in guidance and navigation of an autonomous robot," IEEE Trans. on Robotics and Automation, vol. RA-7, no. 2, pp. 193-204, 1991.

J. Crowley, "Asynchronous control of orientation and displacement in a Robotic Vehicles," Proc. IEEE Int'l Conf. on Robotics & Automation, pp. 1277-1282, 1989.

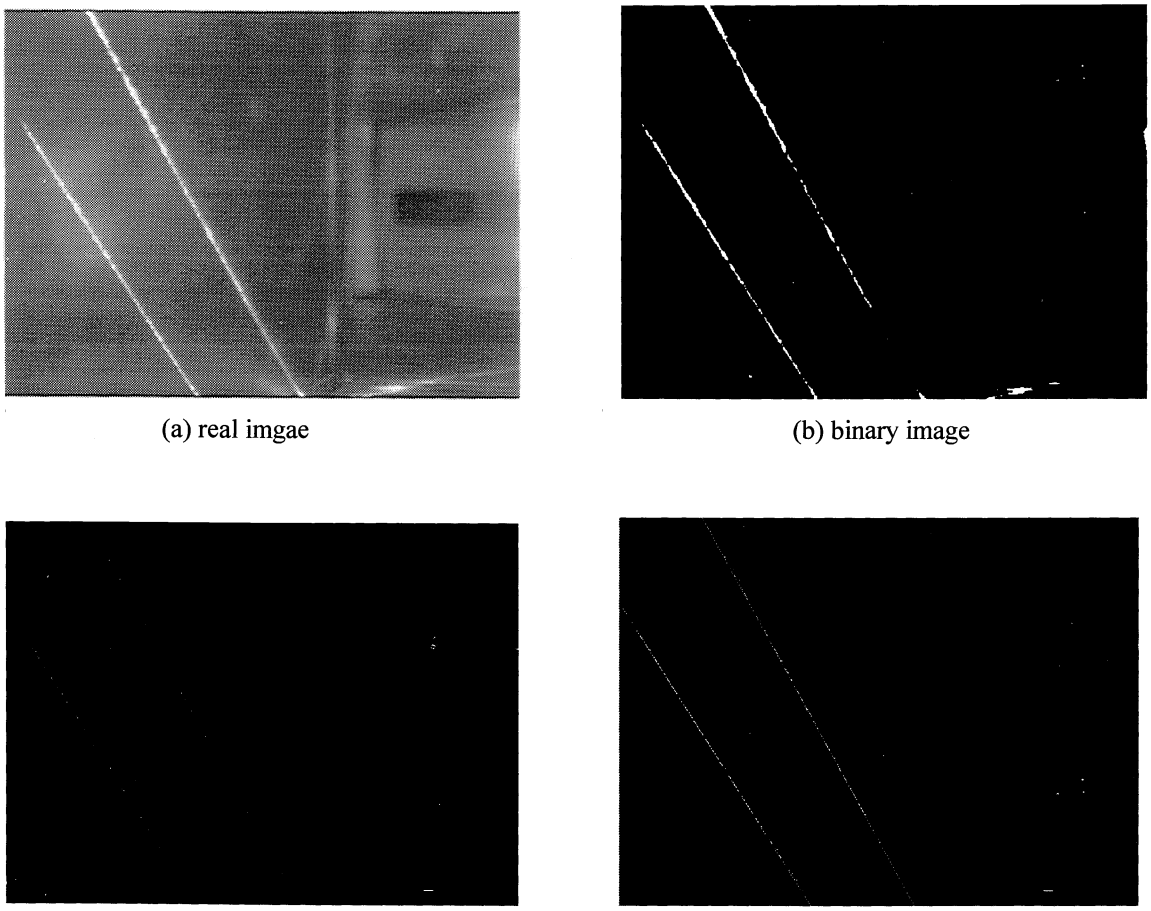

(a) real imgae (b) binary image

(c) thined image (d) result of Hough transform

Fig.8 Results of image processing

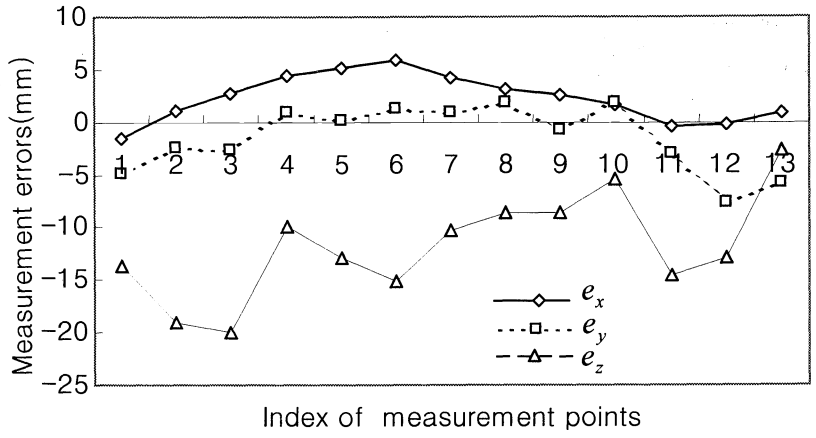

(a) Case of laser source I

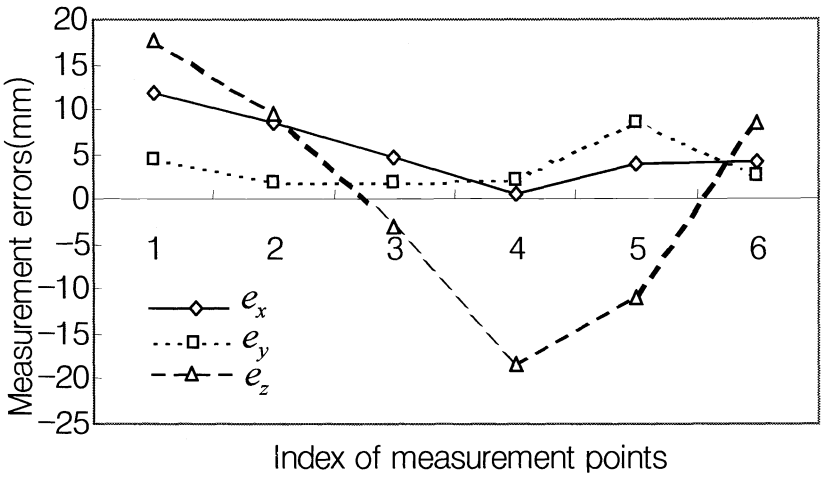

(b) Case of laser Source II

Fig.9 Experimental results of poison estimation

Pixel coordinates		Estimated values			Actual values		
U	V	X	Y	Z	x	y	Z
24	1	98.94	236.56	436.31	100.5	241.5	450.0
68	108	101.13	214.05	530.89	100.0	216.5	55030
84	148	102.71	202.87	580.08	100.0	205.5	600.0
145	150	54.34	182.38	440.11	50.0	181.5	450.0
169	232	55.14	157.56	537.16	50.0	157.5	550.0
177	261	55.92	145.83	584.84	50.0	144.5	600.0
273	334	4.21	109.43	489.73	0.0	108.5	500.0
274	270	3.14	134.25	391.45	0.0	132.5	400.0
275	223	2.52	146.79	341.40	0.0	147.5	350.0
277	73	1.56	171.37	244.56	0.0	169.5	250.0
392	475	-50.35	45.52	485.39	-50.0	48.5	500.0
420	444	-50.16	71.87	387.02	-50.0	79.5	400.0
433	423	-49.13	83.64	347.31	-50.0	89.5	350.0

Table 2. Experimental Data for the right laser source

Pixel coordinates		Estimated values			Actual values		
U	V	X	Y	Z	X	Y	Z
411	117	61.843	164.850	267.792	50.0	160.5	250.0
78	215	58.592	146.368	309.463	50.0	144.5	300.0
107	287	54.536	128.411	347.094	50.0	126.5	350.0
129	341	50.620	111.679	381.730	50.0	109.5	400.0
273	438	3.957	91.898	289.076	0.0	83.5	300.0
278	402	4.212	103.069	258.452	0.0	100.5	250.0

Table 3. Experimental Data for the left laser source

T_{ij}	Laser b1(right side)	Laser b2(left side)
t_{11}	*- 0.417116*	*- 0.158658*
t_{12}	*- 0.002831*	*- 0.039167*
t_{13}	*118.733735*	*63.591918*
t_{21}	*0.513031*	*0.368420*
t_{22}	*- 0.858755*	*- 0.476347*
t_{23}	*248.496339*	*180.585178*
t_{31}	*- 0.031415*	*0.046127*
t_{32}	*- 0.049070*	*- 0.030912*
t_{33}	*480.247345*	*229.079975*
t_{41}	*0.004274*	*0.002966*
t_{42}	*- 0.003704*	*- 0.002330*
t_{43}	*1*	*1*

Table 1. Results of the camera calibration